Original Article

JOURNAL OF REINFORCED PLASTICS & COMPOSITES

Journal of Reinforced Plastics and Composites
32(11) 846–859

DOI: 10.1177/0731684413477711
jrp.sagepub.com

SAGE

Effects of cylindrical and sheet types of nanoparticles on thermal properties and chain folding free energy of poly(ethylene terephthalate)

V Goodarzi[1], A Shadakhtar[2], M Sirousazar[3], M Mortazavi[4] and S Ghaniyari-Benis[5]

Abstract

Poly(ethylene terephthalate) (PET) nanocomposites were prepared through a solution casting method using Multi wall carbon nanotubes (MWCNT) and organically modified montmorillonite (OMMT) as nanoparticles and their morphological and thermal properties investigated. The X-ray diffraction and transmission electron microscopy measurements showed that decreasing the ratio of MWCNT to OMMT for the same amount of OMMT creates better conditions for intercalation of PET macromolecules and promotes the transformation of OMMT nanostructures from the intercalated to exfoliated state. It was concluded that the Ozawa's model was not suitable to interpret the crystallization behavior of the nanocomposites. Based on Liu's model, it was found that the sample containing the lower ratio of MWCNT to OMMT had the highest crystallization rate. Investigation of activation energy and nucleation activity using Vyazovkin's and Dobreva's models revealed that the sample having the smallest ratio of MWCNT to OMMT had the lowest energy absorption and highest nucleation activity.

Keywords

Poly(ethylene terephthalate), nanoparticles, carbon nanotube, crystallization, thermal properties, nucleation activity

Introduction

Preparation of polymer nanocomposites using nanoparticles with different geometrical shapes and aspect ratios is an efficient, useful and low cost way of improving polymer matrix properties.[1–4] Carbon nanotubes (CNT) are a kind of nanoparticle which, due to their unique structural, mechanical and chemical properties, are commonly utilized in production of polymer nanocomposites.[1,5] CNT are also used in preparation of sensors, batteries, and also conductive and semiconductive materials.[6–12] Incorporation of CNT into a polymer matrix causes dramatic improvements in the tensile modulus, impact strength, and resistance against ultra-violet (UV) radiation as well as electrical conductivity of the resultant nanocomposite.[13–16]

Poly(ethylene terephthalate) (PET) is one of the well-known polymers which, because of its excellent physical and chemical properties such as high thermal stability, excellent resistance against wear and chemicals and low water absorption, has found diverse applications.[17] There are few reports on preparation of PET/CNT nanocomposites by a solution casting method.[18,19]

[1]Applied Biotechnology Research Centre, Baqiyatallah University of Medical Sciences, Tehran, Iran
[2]Nanobiotechnology Research Center, Baqiyatallah University of Medical Science, Tehran, Iran
[3]Faculty of Chemical Engineering, Urmia University of Technology, Urmia, Iran
[4]School of Chemical Engineering, University of Tehran, Tehran, Iran
[5]Department of Chemical and Petroleum Engineering, Sharif University of Technology (SUT), Tehran, Iran

Corresponding author:
V Goodarzi, Applied Biotechnology Research Centre, Baqiyatallah University of Medical Science, P.O. Box: 19945-546, Tehran, Iran.
Email: v.goodarzi@hotmail.com

Solution casting is known as a suitable method for preparation of polymer films, but this method is not commercially used.[20,21] In spite of the great importance of PET/CNT nanocomposites,[16] there are only some limited studies on their morphological properties in the open literature.[16,22] Furthermore, little attention has been paid to the synergistic effect among different kinds of nanoparticles on the mechanical, thermal and electrical properties of PET/CNT nanocomposites. Gao et al.[23] studied the effects of functional single wall CNT (SWCNT) and organically modified montmorillonite (OMMT) nanoparticles on the microstructures of polypropylene grafted by maleic anhydride (PP-g-MA) nanocomposites and investigated the synergistic effect between nanoparticles.

In this work, PET nanocomposites were prepared through a solution casting method using MWCNT and OMMT as nanoparticles. The morphological and thermal properties of the prepared samples were investigated using wide angle X-ray scattering (WAXS), transmission electron microscopy (TEM), differential scanning calorimetry (DSC) and thermogravimetric analysis (TGA) techniques. The synergistic effects of MWCNT and OMMT nanoparticles on the thermal properties of PET/MWCNT/OMMT nanocomposites were also studied. Three different models, the Avrami, Ozawa and Liu models,[17] were used to investigate the crystallization kinetics of the prepared nanocomposites. The nucleation activity, surface folding free energy and crystalline activation energy were also calculated on the basis of Dobreva,[37] Hoffman and Vyazovkin theories.[4]

Experimental

Materials

PET was supplied by Tondguyan Petrochemical Co. (Iran) with number average molecular weight of 22.4 kg/mol and weight average molecular weight of 39.5 kg/mol. OMMT, with the commercial name of Closite 10 A (dimethyl benzyl hydrogenated tallow quaternary ammonium (2MBHT) as organomodifier), was purchased from Southern Clay Co. (USA). MWCNT, with 99.9% purity and specific surface area of 200±25 m^2/g were purchased from Carbons21 Co. (Austria). A mixture of 3:1 (vol.%/vol.%) concentrated sulfuric acid/nitric acid was used for MWCNT carboxylation.

Sample preparation

PET was first dissolved in a 3:1 (wt%: wt%) mixture of phenol/chloroform solution. Subsequently, nanoparticles (i.e. MWCNT and OMMT) were added to this solution and the mixture was ultrasonicated at ≈200 W for 15 min at 70°C to obtain a homogenous mixture. Then that mixture was cast in petri dish and was maintained 5 min it room temperature for extraction of air bubbles. Finally, the solvent was extracted from the cast films using a vacuum oven at 50°C for 24 h. The final compositions of the prepared samples have been shown in Table 1.

Table 1. Composition of the studied samples.

Sample code	MWCNT (wt%)	OMMT (wt%)
PET	–	–
PET-S0.5M1	0.5	1
PET-S1M1	1	1
PET-S1.5M1	1.5	1

MWCNT: multi wall carbon nanotube; OMMT: organically modified montmorillonite; PET: poly(ethylene terephthalate).

Characterizations

WAXS analysis was performed using a Philips diffractometer (PW 2400, Netherlands) operating at 40 kV and 30 mA with Cu-Kα radiation ($\lambda = 0.154$ nm). TEM observations were performed using a CEM902A Zeiss (Cheek) instrument on microtomed specimens approximately 50 nm thickness. DSC was carried out using a TA Instruments Q200, (USA) differential scanning calorimeter. Samples having approximately 5 mg weight were heated to 320°C by heating rate of 10°C/min under nitrogen atmosphere and held for 5 min to remove any residual nuclei before cooling at the specified cooling rates of 2.5, 5, 10 and 20°C/min. TGA was performed at multiple heating rates of 5, 10 and 20°C/min from room temperature (25±1°C) to 700°C under nitrogen atmosphere using a TA Instruments Q500, (USA). SEM observations were performed using a Philips electron microscope (CM200, Netherlands).

Results and discussion

WAXS analysis

Figure 1(a) depicts the WAXS patterns of OMMT clay and prepared ternary nanocomposite samples. The (001) plane crystalline structure of OMMT was observed at $2\theta = 4.8^\circ$ ($d = 19.2$ Å). According to Figure 1(a), it can be clearly seen that the PET-S1.5O1 nanocomposite has a characteristic peak around 3.7° ($d = 24.9$ Å). This decrease in 2θ value means that the OMMT layers in PET-S1.5O1 nanocomposite were mainly intercalated by PET macromolecules. On the other hand, the WAXS pattern of PET-S1O1 showed a characteristic diffraction peak at 2.1° ($d = 29.9$ Å). It can be deduced that decreasing the

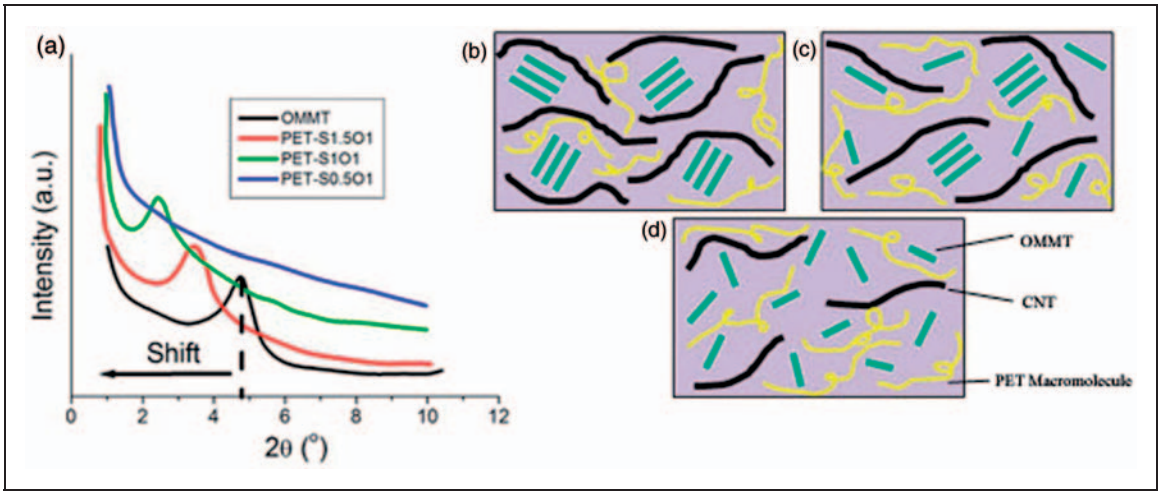

Figure 1. (a) XRD patterns of prepared samples, schematic representation of ternary nanocomposites; (b) PET-S1.5O1; (c) PET-S1O1; and (d) PET-S0.5O1.
XRD: X-ray diffraction; PET: poly(ethylene terephthalate).

amount of MWCNT nanoparticles created better conditions for intercalation of PET macromolecules in the OMMT galleries and promoted the transformation of OMMT nanostructures from the intercalated to a partially exfoliated state because decreased the motion of PET macromolecules. Similar result has been discussed previously by Gao et al.[23] for PP-g-MA/MWCNT/OMMT nanocomposites. However, the PET-S0.5O1 nanocomposite showed no peak in WAXS that indicated a better nanostructure compared to the other samples. It could be attributed to the synergistic effect of simultaneous incorporation of both MWCNT and OMMT nanoparticles. In this case, the OMMT platelets were mainly exfoliated because the MWCNT nanoparticles and PET macromolecules enter into the interlayer galleries of OMMT. The intercalation of PET macromolecules in lower amounts of MWCNT nanoparticles occurred easily. Therefore, MWCNT nanoparticles could assist the PET macromolecules to improve the nanostructure. A schematic representation of the role of MWCNT nanoparticles in diffusion of PET macromolecules to interlayers, of OMMT and dispersion of OMMT layers in the ternary nanocomposites is shown in Figure 1(b) to (d).

TEM observations

The dispersion of OMMT and MWCNT in PET-S1.5O1 and PET-S1O1 nanocomposites is presented in Figure 2. As seen, in the PET-S1.5O1 nanocomposite the length of the MWCNT bundles were in the nanometric scale, about 50 nm, with no selective orientation (Figure 2(a) and (b)). The PET-S1O1 sample also showed a good dispersion state of the MWCNT (Figure 2(c) and (d)). This direct observation supports the result of previous discussion on WAXS results showing the nanostructured morphology for PET-S1O1 sample.

Nonisothermal crystallization behavior

Figure 3 shows the DSC curves for the PET-S0.5O1 nanocomposite sample. The degree of crystalline X_c was calculated based on the crystallization enthalpy ΔH_c values, which in turn was calculated based on the normalized PET fraction. The thermodynamic contributions of MWCNT and OMMT nanoparticles to the enthalpy were neglected. The crystallization enthalpy of 100% crystalline PET (ΔH_c^o) was obtained from elsewhere.[24] Useful parameters such as onset crystallization temperature (T_o), crystallization temperature at exothermic peak (T_p) and final crystallization temperature (T_∞) were obtained from DSC curves. T_p and X_c values related to the PET matrix of the prepared nanocomposites are presented in Table 2. T_p increased with incorporation of nanoparticles into the PET matrix. It can also be seen that by increasing the cooling rate the crystallization temperature decreased. At lower cooling rates, there is enough time for the crystallite nucleation process and thus T_p shifts to higher temperatures.[25] Figure 4 shows the change of T_p on increasing the cooling rate. It is obvious from this figure that T_p values for ternary nanocomposites samples increased with decreasing the ratio of MWCNT to OMMT. This phenomenon could be attributed to better dispersion of nanoparticles in nanocomposites and increased heterogeneous nucleation created by MWCNT and OMMT platelets nanoparticles. PET macromolecules could easily attach to the modified surfaces of OMMT and MWCNT nanoparticles which

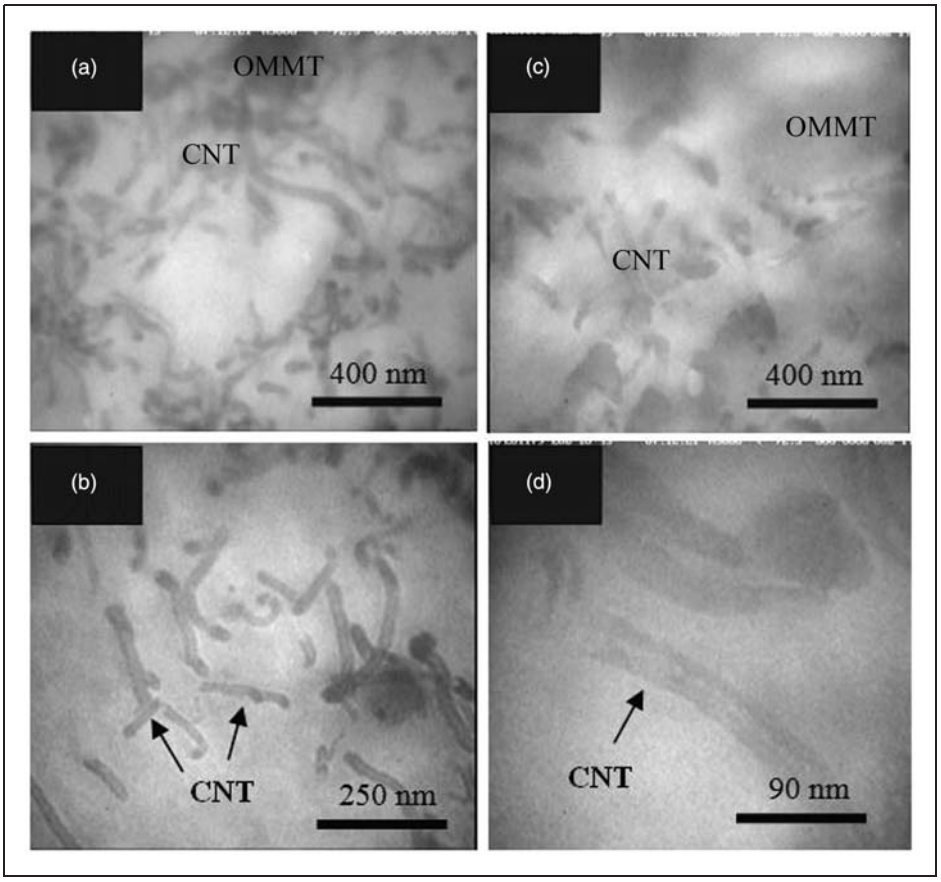

Figure 2. TEM images of ternary nanocomposites: (a,b) PET-S1.5O1 and (c,d) PET-S1O1.
TEM: transmission electron microscopy; PET: poly(ethylene terephthalate).

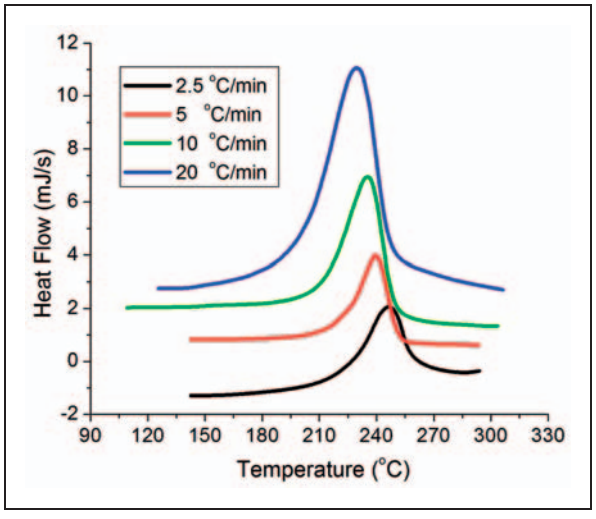

Figure 3. DSC thermograms at different cooling rate of the PET-S0.5O1 sample.
DSC: differential scanning calorimetry; PET: poly(ethylene terephthalate).

this facilitates the crystallization of PET at higher temperatures.[23,26,27]

Nonisothermal crystallization kinetics

Crystallization kinetics can provide a precise understanding of the crystallization behavior of nanocomposites. Using dynamic crystallization measurements, exothermic crystallization data can be obtained as a function of temperature and heat flow (dH_c/dT) for any cooling rate. Relative crystallinity as a function of temperature, X_T, for PET-S1O1 is presented in Figure 5. A curvature of the X_T curve versus temperature for this sample reveals the effect of cooling rate on the crystallization process. Using the relationship between time and temperature in a nonisothermal crystallization process, T values on x-axis can be converted to t values, as shown in Figure 5(b). The obtained results are tabulated in Table 3. The half crystallization time $t_{1/2}$ is defined as the 50% of maximum crystallinity time. It is observed that $t_{1/2}$ decreases with increasing the cooling rates. In addition, $t_{1/2}$ for ternary nanocomposites was lower than pure PET. It was observed that

Table 2. Crystallization parameters of the studied samples at different cooling rates.

Sample	2.5°C/min			5°C/min			10°C/min			20°C/min		
	T_p (°C)	ΔH_c (J/g)	X_c (%)	T_p (°C)	ΔH_c (J/g)	X_c (%)	T_p (°C)	ΔH_c (J/g)	X_c (%)	T_p (°C)	ΔH_c (J/g)	X_c (%)
PET	228	56.7	42.0	224	51.2	37.9	219	49.6	36.8	217	41.3	30.6
PET-S1.5O1	234	48.8	36.1	230	43.1	31.9	224	41.5	30.7	220	33.3	25.1
PET-S1O1	241	44.5	32.9	238	40.1	29.7	233	46.8	34.7	227	34.8	25.8
PET-S0.5O1	245	49.2	36.4	238	48.0	35.5	236	47.9	35.5	229	47.4	35.1

PET: poly(ethylene terephthalate).

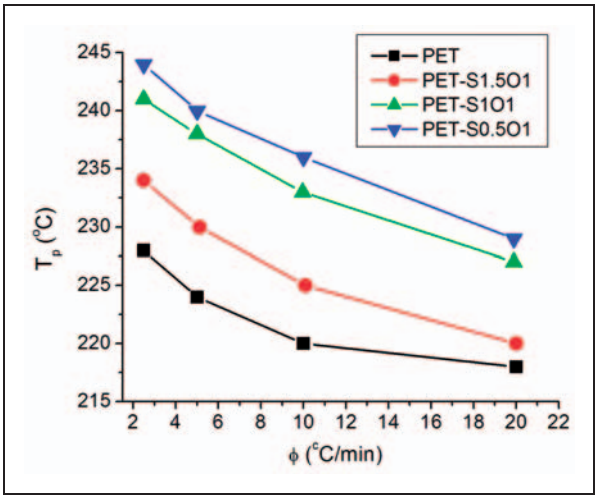

Figure 4. Maximum crystallization temperature of samples vs. cooling rate.

simultaneous incorporation of MWCNT and OMMT increased the crystallization rate due to heterogeneous nucleation, which facilitated the crystallization process.

Nonisothermal crystallization kinetics by using the Avrami model

The kinetics of an isothermal crystallization process can be studied by Avrami's method at a constant temperature.[28] Equation (1) is the Avrami equation to calculate the degree of crystallinity at any given time

$$1 - X(t) = \exp(-Z_t t^n) \quad (1)$$

where $X(t)$ is the degree of crystallization at time t, Z_t is Avrami's constant characterizing the crystallization rate and n is Avrami's exponent. The Avrami equation gives some information about crystallization behavior by using the Z_t and n parameters. Z_t is a function of temperature which gives information about crystallite nucleation rate and diffusion of polymer macromolecules for making crystallite structures. n is a measure

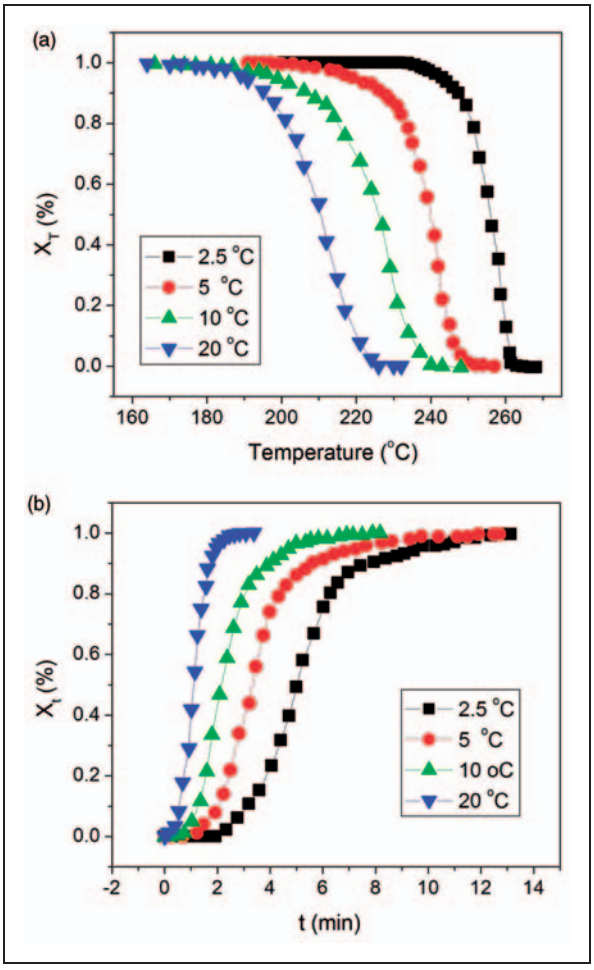

Figure 5. Plots of relative crystallization at different cooling rates vs.: (a) temperature and (b) time for PET-S1O1 sample. PET: poly(ethylene terephthalate).

of crystallite growth (one-, two- or three-dimensional growth) describing the nucleation mechanism (homogeneous or heterogeneous).[29] The double logarithmic form of equation (1) yields

$$\ln(-\ln[1 - X_T]) = \ln Z_t + n \ln t \quad (2)$$

Table 3. Nonisothermal crystallization behavior for the studied samples.

Samples	φ (°C/min)	T_p (°C)	t (min)	$t_{1/2}$ (min)
PET	−2.5	228	7.2	5.1
	−5	224	5.1	4.0
	−10	219	2.9	2.5
	−20	217	1.3	1.4
PET-S1.5O1	−2.5	234	3.4	4.9
	−5	230	1.5	3.9
	−10	224	0.9	2.4
	−20	220	0.5	1.4
PET-S1O1	−2.5	241	3.7	4.8
	−5	238	1.9	3.3
	−10	233	1.4	2.2
	−20	227	0.7	1.1
PET-S0.5O1	−2.5	245	3.6	4.9
	−5	240	1.5	3.9
	−10	236	0.9	2.4
	−20	229	0.5	1.3

PET: poly(ethylene terephthalate).

Fitting experimental data to equation (2), n and Z_t values can be calculated from the slope and intercept of plots of $\ln[-\ln(1-X_T)]$ against $\ln t$ at each cooling rate, as shown in Figure 6. It should be noticed that in these calculations, n and Z_t do not have same physical meaning in isothermal and nonisothermal crystallization due to in nonisothermal crystallization total phenomena dependence on the cooling rate. Thus, Jeziorny proposed that Z_t is affected by φ (is cooling rate) and should be modified to Z_c.[30]

The results of Avrami and Jeziorny models are presented in Table 4. n depends on molecular weight, nucleation type and secondary crystallization regime and is not affected by temperature.[31] Simultaneous addition of MWCNT and OMMT nanoparticles changed the n parameter which reveals a heterogeneous nucleation. Also, Z_t had higher value for PET-S0.5O1 sample compared to the PET-S1.5O1 sample. This is attributed to the better dispersion and distribution of MWCNT and OMMT nanoparticles in the PET matrix as discussed previously by TEM and WAXS results.

Nonisothermal crystallization kinetics by the Liu model (modified Avrami–Ozawa models)

Liu et al.[34,35] developed a new method to investigate nonisothermal crystallization kinetics by combining the Avrami and Ozawa models, it has been extensively used in nanoisothermal crystallization analysis of many polymer systems. In this model, crystallization degree is correlated to φ and t. Their equation can be rearranged as the following equation, for a constant value of X_t

$$\ln \varphi = \ln F(T) - \alpha \ln t \tag{3}$$

In equation (3), the kinetic parameter, $F(T) = \left[\frac{K_o^{no}}{K_a^{na}}\right]^{\frac{1}{no}}$, is the cooling rate required to reach a determined degree of crystallization and $\alpha = \frac{n_a}{n_o}$ is the ratio of Avrami's exponent to Ozawa's exponent that depends on the dimensions of crystal growth. According to equation (3), at a constant degree of crystallinity, a plot of $\ln \varphi$ versus $\ln t$ should be a linear curve that $F(T)$ and α can be obtained from its slope and intercept, respectively. Plots of $\ln \varphi$ versus $\ln t$ are shown in Figure 6(c) at different degrees of crystallinity. These curves are linear, which show the validity of Liu's model in interpreting the dynamics of crystallization for our studied samples. The values of $F(T)$ and α were determined for each nanocomposite and are presented in Table 5. The value of α varied between 1.22 and 1.34 for PET-S0.5O1 nanocomposite and it had inversed dependence to the ratio of MWCNT to OMMT. The higher value of α for the PET-S0.5O1 sample compared to the other samples is attributed to a better synergistic effect between MWCNT and OMMT nanoparticles on crystallization of the PET matrix. This observation is related to the faster crystallization of the PET-S0.5O1 sample compared to the other ones.

Nucleation activity

The effect of heterogeneous crystallite nucleating agents on polymer matrix crystallization behavior has been investigated by Dobreva et al.[36] The nucleation activity of a heterogeneous nucleating agent (ψ) is a factor on which the activity of a heterogeneous nucleating agent can be judged. If the introduced particles in a polymer matrix are active to enhance the crystallization process of the matrix, ψ approaches zero, but if they are neutral, ψ approaches 1. The particle activity coefficient is defined as $\psi = B^*/B$ in which B^* and B can be determined from the following equations[4–37]

$$\ln \psi = Const - \frac{B}{\Delta T_P^2} \quad \text{For homogenous nucleation}$$
$$\ln \psi = Const - \frac{B^*}{\Delta T_P^2} \quad \text{For heterogeneous nucleation} \tag{4}$$

In this equation, $\Delta T_P = T_m - T_p$ is the super cooling amount. Figure 7(a) depicts $\ln \varphi$ curves versus $1/\Delta T_P^2$ for all of the studied samples. The correlation coefficient (R^2) was higher than 0.96. According to equation (4), the slope of the curves gives B^* values.

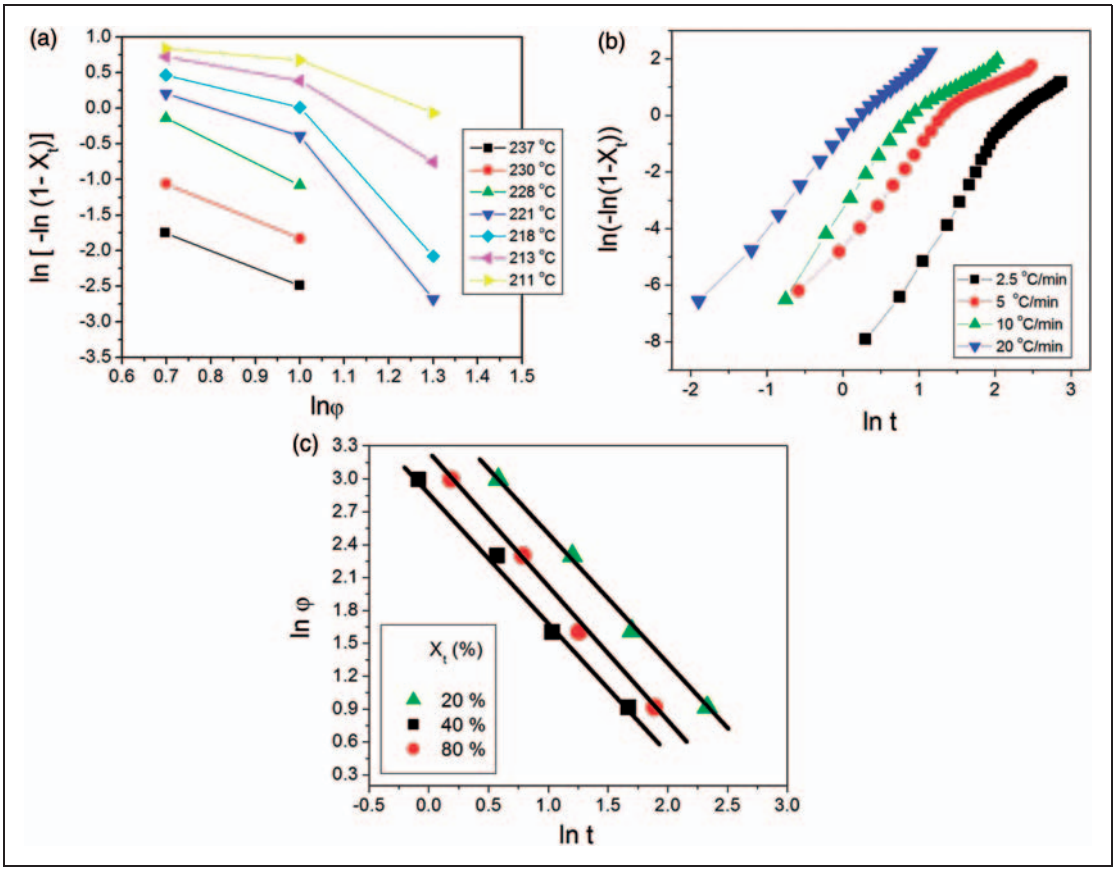

Figure 6. Plots of: (a) ln[−ln(1−X_t)] vs. ln φ (Ozawa model); (b) ln[−ln(1−X_t)] vs. ln t (Avrami model); and (c) ln φ vs. ln t (Liu model) at a constant degree of crystallization in nonisothermal crystallization mode for PET-S0.5O1 sample.
PET: poly(ethylene terephthalate).

Table 4. Nonisothermal crystallization parameters obtained from Avrami and Jeziorny's methods.

Sample	φ (°C/min)	n	Zt
PET	−2.5	3.1	0.06
	−5	3.2	0.08
	−10	3.3	0.36
	−20	3.5	0.66
PET-S1.5O1	−2.5	2.9	0.09
	−5	3.0	0.10
	−10	2.1	0.41
	−20	2.8	0.68
PET-S1O1	−2.5	3.0	0.11
	−5	3.2	0.12
	−10	3.3	0.43
	−20	3.4	0.69
PET-S0.5O1	−2.5	2.8	0.10
	−5	3.1	0.13
	−10	3.5	0.42
	−20	3.7	0.73

PET: poly(ethylene terephthalate).

Table 5. Crystallization kinetic parameters at different crystallization degrees using Liu model for the studied samples.

Sample	X_t (%)	ln $F(T)$	α
PET	20	2.94	1.16
	40	3.25	1.23
	80	3.76	1.21
PET-S1.5O1	20	2.92	1.18
	40	3.22	1.25
	80	3.74	1.23
PET-S1O1	20	2.67	1.20
	40	3.43	1.26
	80	3.54	1.24
PET-S0.5O1	20	3.02	1.22
	40	3.19	1.26
	80	3.67	1.34

PET: poly(ethylene terephthalate).

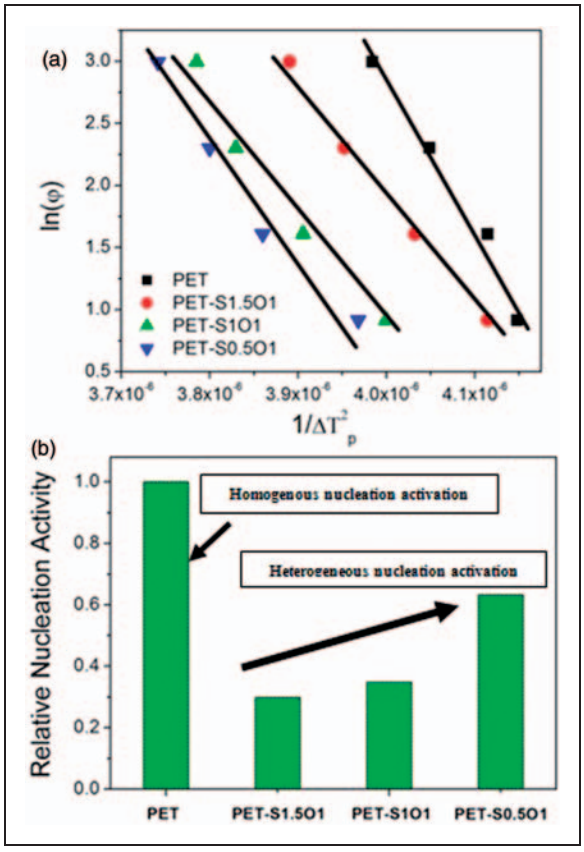

Figure 7. Plots of: (a) ln φ vs. $1/\Delta T_p^2$; (b) relative nucleation activation for studied samples.

Accordingly, Figure 7(b) gives the ratio of B^* parameter for the studied samples with respect to pure PET (B^* supposed to be 1). It can be seen from Figure 7(b) that the amount of nucleation activity for the ternary nanocomposites increased with incorporation of low ratio of MWCNT the PET matrix. Also, it is observed that the sample having the lowest value of the MWCNT to OMMT ratio (PET-S0.5O1 sample) had the highest nucleation activity value (ψ).

Crystal growth, surface folding free energy and lamellar thickness

Thermodynamics and crystallization kinetics can be investigated using the Hoffman-Lauritzen theory.[38,39] According to this theory, the amount of crystal growth (G) as a function of temperature is determined as follows

$$G = G_o \exp\left(\frac{-U*}{R(T_o - \varphi t - T_\infty)}\right) \times \exp\left(\frac{-K_g}{(T_o - \varphi t)\left[T_m^o - (T_o - \varphi t)\right]f}\right) \quad (5)$$

where G is the growth rate of crystalline spherulites estimated by $(t_{1/2})^{-1}$,[40] G_0 is a power law pre-factor, and $f = 2(T_o - \varphi t)/\left(T_m^o + (T_o - \varphi t)\right)$is a modifying factor in this equation. U^* and T_∞ are Vogel–Fulcher–Tamman–Hesse ($VFTH$) parameters that are defined based on the polymer segmental translation in liquid/crystal middle phase conditions. Values of the $VFTH$ universal constants are U^*=6300 J/mol, which is the activation energy of segmental folding under cooling conditions and $T_\infty = T_g - 30$(K) is hypothetic temperature at which the motion occurs by use of viscous flow.[39] $T_g = 80^\circ$C and the equilibrium melting temperature T_m^o=280°C for neat PET were obtained from the literature.[41] These values were determined by Marand et al.[42] using the Hoffman–Weeks extrapolation.[43] Thus, the equilibrium fusion temperature T_m^o was obtained as shown in Figure 8(a). K_g is the nucleation parameter related to the required energy of lamellae lateral and entangled aspect. This parameter is defined as follows[39]

$$K_g = \frac{j\left(0.11\sqrt{a_o b_o}\right) b \sigma_e T_m^o}{k_B} \quad (6)$$

where $b = 5.53$ Å is the distance between two-fold surfaces, a_0 and b_0 are dimensional parameters of a PET unit cell having the values of $a_0 = 4.57$ Å and $b_0 = 5.95$ Å.[44] σ_e is the surface free folding energy, k_B is the Boltzman constant, and j determines the crystallization regime. In this study, it was assumed that second Hoffman's regime exists and therefore $j = 2$. Using equation (6) and isoconvetional method (average temperature) for nonisothermal crystallization, K_g was calculated for different samples. Plots of $\ln G + U^*/(R(T_c - T_\infty))$ versus $((T_o - \varphi t)[T_m^o - (T_o - \varphi t)]f)^{-1}$ are shown in Figure 8(b). The slopes of linear curves give the values of K_g. Using K_g and equation (6), σ_e was calculated and is tabulated in Table 6. The calculated values are extremely close to the values obtained from the isoconventional method. It is shown that decreasing the ratio of MWCNT to OMMT nanoparticles causes the σ_e to decrease. Reduction in σ_e increases the entanglement entropy of crystallite lamellae and therefore decreases their homogeneity and disorders entangled surfaces. Simultaneous incorporation of MWCNT and OMMT decreases the energy level for formation of new surfaces and thus increases the crystallization rate. Using a thermodynamic approach, the crystallite lamellae thickness could be calculated according to the following equation[45]

$$T_m = T_m^o\left(1 - \frac{2\sigma_e}{\Delta H_f L}\right) \quad (7)$$

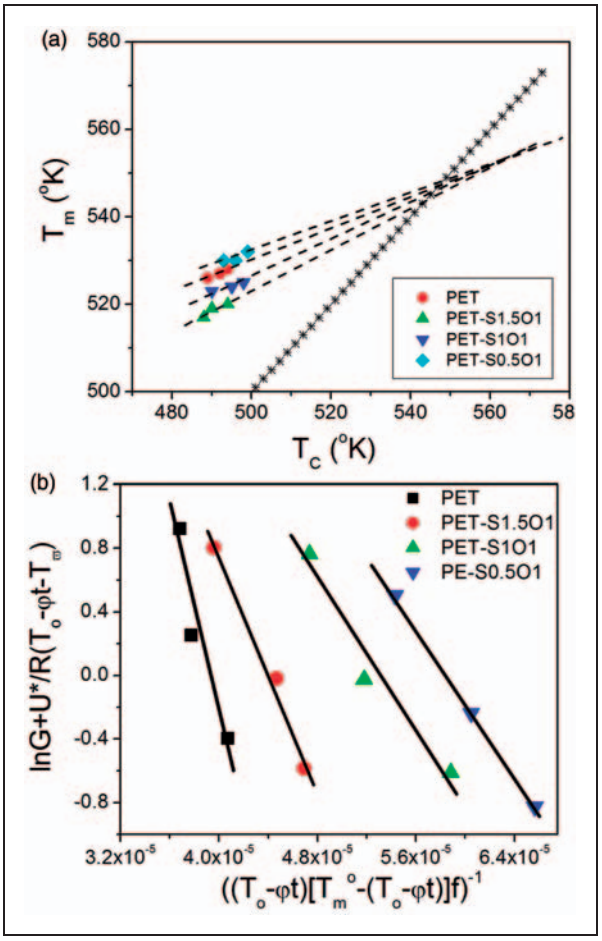

Figure 8. Plots of: (a) Hoffman–Weeks plot; (b) ln $G+U^*/(R(T_c-T_\infty))$ curves vs. $((T_o-\varphi t)[T_m^o-(T_o-\varphi t)]f)^{-1}$.

where T_m^o is the equilibrium melting temperature, σ_e is the surface energy of the crystalline spherulites, L is lamella thickness and ΔH_f is the fusion enthalpy of 100% crystalline polymer. Based on equation (5), the lamella thickness was calculated for the studied samples and is presented in Table 6. It is observed that incorporation of a lower ratio of MWCNT to OMMT into PET matrix increases the thickness of the lamella. Increasing the surface energy of the lamella further increases the distance between crystalline layers and this is the reason for the increase in thickness of the lamella.

Effective activation energy for nonisothermal crystallite growth

Mathematical methods are commonly employed to study the amount of required energy to reach a determined crystallinity degree. For example, the Kissinger method is a general way to calculate the activation energy of crystallization under nonisothermal conditions.[46] However, Vyazovkin and Sbirazzuli[47,48] showed that this method was not valid when applied to the processes of melt crystallizations. Friedman[49] presented a method to investigate the effective activation energy using non-isothermal crystallization data. The following equation shows the formula to obtain the activation energy E_a at each degree of crystallization

$$\left(\mathrm{d}X/\mathrm{d}t\right)_X = k_0 \exp\left(-\frac{\Delta E_X}{RT_X}\right) \tag{8}$$

where X is the crystallization conversion, $\mathrm{d}X/\mathrm{d}t$ is the instantaneous crystallization rate as a function of time at a constant degree of crystallization conversion and X_t is the sum of crystallization under curve at different cooling rates. Plotting the right side of equation (8) versus $1/T_x$ results in a linear curve where its slope is equal to $\Delta E_x/R$. Linear curves of $\ln(\mathrm{d}X/\mathrm{d}t)$ versus $1/T_x$ were obtained at different relative crystallinity degrees. For all samples the correlation parameter was obtained around 0.980. The dependency of the effective activation energy of the samples to the relative crystallization degrees is presented in Figure 9(a). It is observed that ΔE increased with crystallinity. Although, in the case of PET-S0.5O1, the trend is ascending until $X_t<20\%$ and after that the trend was descending. These trends are attributed to the decrease of effective energy due to the effective heterogeneous nucleation as discussed previously in the nonisothermal crystallization kinetics section. Also, it can be seen that at $X_t<60\%$, the required energy was higher for samples containing lower ratios of MWCNT to OMMT. In addition, effective barrier energy was obtained as a function of temperature at constant crystallinity degree and is shown in Figure 9(b). The PET-S1.5O1 sample has the lowest activation energy, while the PET-S0.5O1 sample had the highest. It could be mentioned that low ratio of MWCNT to OMMT causes some limitation of translation and thus high level of energy is required for macromolecular segments to deposit in crystallite lamellae. Figure 9 also gives the Lauritzen–Hoffman's parameters, i.e. K_g and U^*. According to the equation presented by Vyazovkin and Sbirazzuli,[50] based on the Hoffman theory, the activation energies required for crystallization can be calculated without knowing the required energy of nucleation and growth. The dependency of the effective activation energy on temperature is defined as follows

$$E_a(T) = U^* \frac{T^2}{(T-T_\infty)^2} + K_g R \frac{T_m^o 2 - T^2 - T_m^0 T}{(T_m^0 - T)^2 T} \tag{9}$$

K_g can be calculated by nonlinear fitting of experimental data using equation (9) on the basis of the Levenberg–Marquardt method. The estimated values

Table 6. Surface folding free energy (σ_e), kinetic parameter (K_g) and lamellae thickness (L) under different crystallization processes.

Sample	K_g^a (K^2)	σ_e^a (mJ/m^2)	L^a (Å)	K_g^b (K^2)	σ_e^b (mJ/m^2)	L^b (Å)
PET	2.63×10^5	79.3	227	2.62×10^5	77.0	225
PET-S1.5O1	1.85×10^5	74.2	182	1.86×10^5	73.5	179
PET-S1O1	1.56×10^5	62.3	161	1.52×10^5	62.5	163
PET-S0.5O1	1.27×10^5	50.6	142	1.24×10^5	50.9	144

[a]Isothermal crystallization.
[b]Isoconversional approach.
PET: poly(ethylene terephthalate).

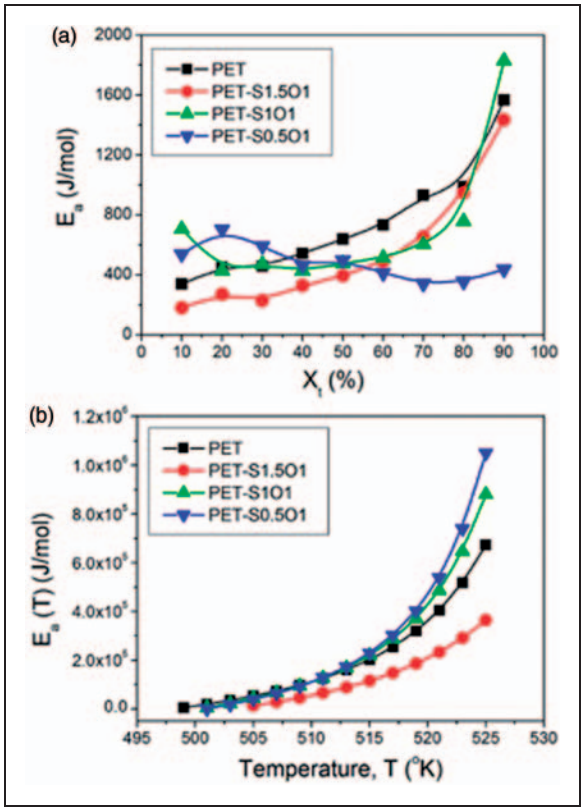

Figure 9. Effective crystallization energy of samples vs.: (a) relative crystallinity; and (b) average temperature.

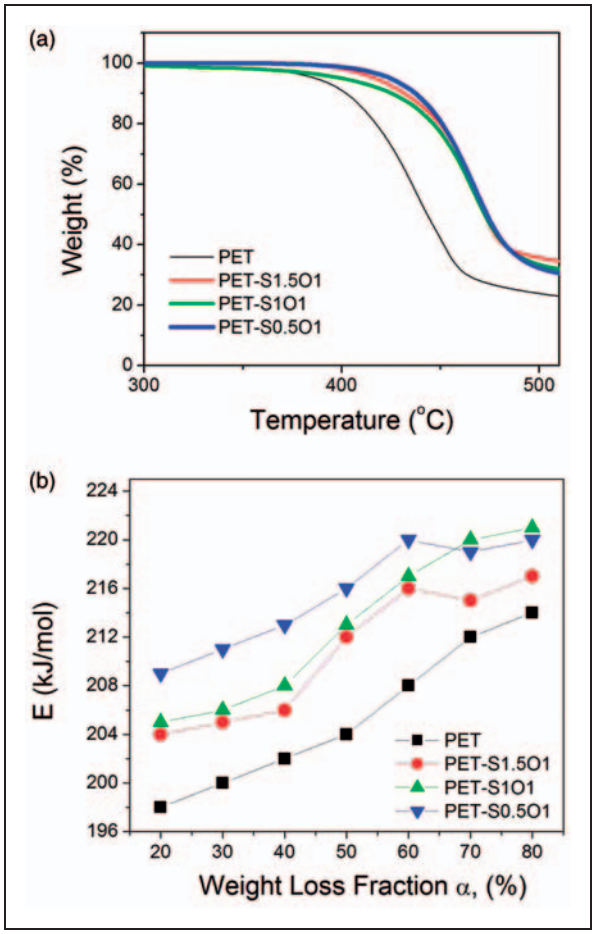

Figure 10. (a) TGA thermograms at heating rate of 10°C/min; (b) variation of activation energy against energy conversion degree in N_2 atmospheres.
TGA: thermogravimetric analysis.

using this method are presented in Table 6. These values, which are used to determine the surface free folding energy according to equation (6), are very close to previously reported data for isothermal crystallization condition. Therefore, isoconventional method can be considered as a successful method to predict the nonisothermal crystallization behavior of PET ternary nanocomposites.

Thermal degradation

Figure 10(a) shows the TGA thermograms of the studied samples. As shown, the thermal stability of the samples increased with decreasing the ratio of MWCNT to OMMT. Based on the X-ray diffraction (XRD) and TEM results, it was deduced that decreasing the ratio of MWCNT to OMMT promotes the diffusion of PET macromolecules to OMMT galleries and changes the intercalated morphology to exfoliated one.

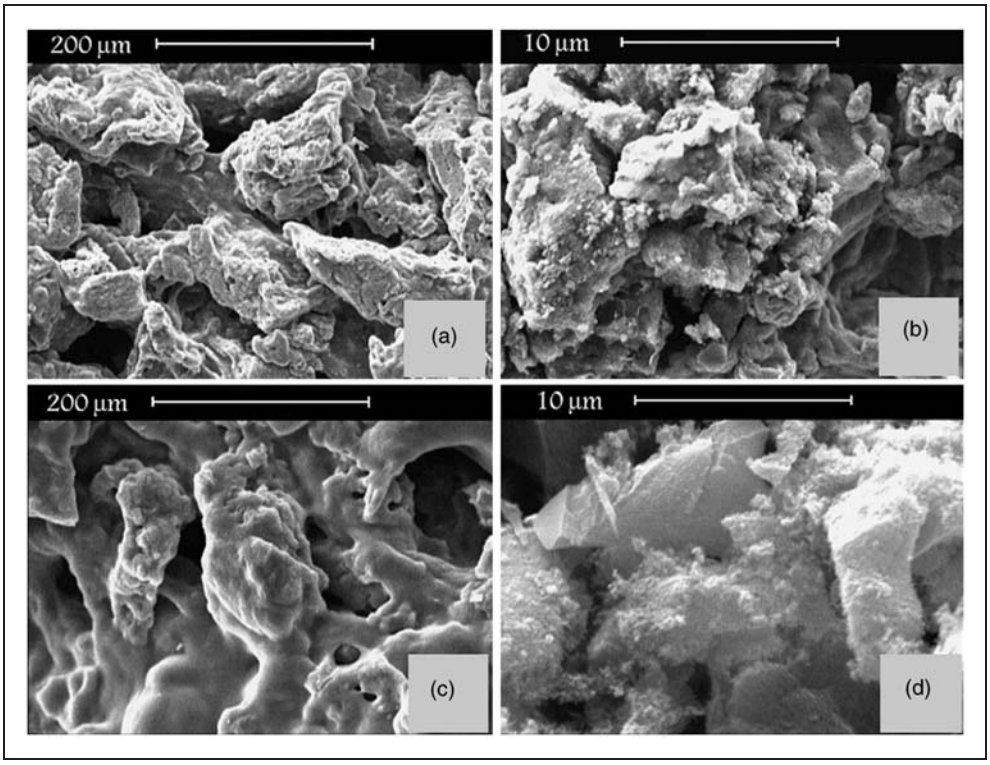

Figure 11. SEM images of charred residue for ternary nanocomposites: (a,c) PET-S1.5O1 and (b,d) PET-S0.5O1 samples.
SEM: scanning electron microscopy; PET: poly(ethylene terephthalate).

Therefore, incorporating of a lower ratio of MWCNT to OMMT creates a network structure and forms a barrier structure to hinder mass transfer from solid to gas phases.[51,52] It is observed that PET had the lowest thermal stability compared to the other studied samples. Decreased thermal stability for samples with higher ratio of MWCNT to OMMT is attributed to the reduced aspect ratio of MWCNT during the acid treatment procedure that induces defects on MWCNT structure.[53] Figure 10(b) shows the values of activation energy obtained from the Flynn model of degradation at 20–80% conversion in nitrogen atmospheres. It is observed that incorporation of 0.5 wt% MWCNT and 1 wt% OMMT into PET matrix significantly increased the activation energy. This indicates that this sample had high stability in N_2 atmosphere. The observed increasing trend of E_a with increasing the conversion degree is due to the fact that as the degradation process continues there is formation of free radical during the degradation process. Figure 10(c) and (d) depicts the reaction rate of conversion versus temperature and fitting of the Autocatalytic and Friedman models for PET-S0.5O1 sample at different heating rates under N_2 atmosphere. The fitting method of Autocatalytic and Friedman models has been mentioned elsewhere.[54,55] Using these models, it can be inferred that Friedman model has the best fitting to the experimental data.

Charred residue morphology

Figure 11 exhibits the charred residue morphology of PET-S1.5O1 and PET-S0.5O1 samples at different magnifications. The surface char of the PET-S1.5O1 sample was more rough and porous compared to the PET-S0.5O1 sample. It can be deduced that the sample having lower ratio of MWCNT to OMMT showed lower porosity and higher thermal stability. Unusual crystalline structures were observed in these samples. It seems that OMMT nanoparticles in the presence of MWCNT along with network structures of degraded PET macromolecules contribute to the formation of these structures.

Conclusions

The effect of simultaneous incorporation of functional MWCNT and OMMT into PET matrix on thermal properties of ternary PET/MWCNT/OMMT nanocomposites was studied. Investigation of nanostructure using XRD and TEM techniques showed that by decreasing the ratio of MWCNT to OMMT, exfoliated

morphology can be formed. It was observed that Ozawa's model did not authenticate for investigation of crystallization kinetics of ternary nanocomposites. It was found that the sample containing lower ratio of MWCNT to OMMT has the highest crystallization rate compared to the other samples. Analysis of surface energy of entangled lamellae using Hoffman–Lauritzen theory demonstrated that incorporation of MWCNT and OMMT into PET matrix increases this energy and decreases the crystallite lamellar thickness from 227 Å to 142 Å for PET and PET-S0.5O1, respectively. Investigation of crystallization activation energy using Friedman model showed that activation energy is increased for all studied samples with increasing the crystallization degree. Especially, in the case of sample incorporated with 0.5 wt% of MWCNT and 1 wt% of OMMT this energy is decreased due to non-uniform nucleation phenomenon. Investigation of activation energy at crystallization temperature region using Vyazovkin Sbirazzuli's model revealed that PET-S0.5O1 sample has the highest energy absorption. It was attributed to improved dispersion state of nanoparticles, which might increase the viscosity of PET matrix and consequently confine the PET macromolecular motions. TGA results showed that addition of MWCNT and OMMT prevents the degradation of PET matrix. Additionally, based on the Flynn model it was found that the PET-S0.5O1 sample has the highest activation energy 220 kJ/mol from 20% to 60% of conversion. However, Friedman model was a good fitting for kinetics degradation. Charred residue morphology showed that PET-S0.5O1 sample formed an enhanced microstructure acting as a good barrier against heat and mass transfer having suitable thermal stability.

Acknowledgments

The authors wish to thank the IBB laboratory of Tehran University and Tarbiat Modares University for TEM, and XRD tests.

Funding

This research received no specific grant from any funding agency in the public, commercial, or not-for-profit sectors.

References

1. Sahoo NG, Rana S, Cho JW, et al. Polymer nanocomposites based on functionalized carbon nanotubes. *Prog Poly Sci* 2010; 35: 837–867.
2. Kiliaris P and Papaspyrides CD. Polymer/layered silicate (clay) nanocomposites: An overview of flame retardancy. *Prog Polym Sci* 2010; 35: 902–958.
3. Goodarzi V, Monemian SA, Maleki F, et al. In situ radical copolymerization in presence of surface-modified TiO_2 nanoparticles: influence of a double modification on properties of unsaturated polyester (UP) nanocomposites. *J Macromol Sci Phys* 2008; 47: 472–484.
4. Njuguna J, Pielichowski K and Desai S. Nanofiller-reinforced polymer nanocomposites. *Polym Adv Tech* 2008; 19: 947–959.
5. Iijima S. Helical microtubules of graphitic carbon. *Nature* 1991; 354: 56–58.
6. Schartel B, Pötschke P, Knoll U, et al. Fire behaviour of polyamide 6/multiwall carbon nanotube nanocomposites. *Eur Polym J* 2005; 41: 1061–1070.
7. Ramaratnam A and Jalili N. Reinforcement of piezoelectric polymers with carbon nanotubes: pathway to next-generation sensors. *J Intell Mater Syst Struct* 2006; 17: 199–208.
8. Park C, Kang JH, Harrison JS, et al. Actuating single wall carbon nanotube–polymer composites: intrinsic unimorphs. *Adv Mater* 2008; 20: 2074–2079.
9. Deshmukh S and Ounaies Z. Single walled carbon nanotube (SWNT)-polyimide nanocomposites as electrostrictive materials. *Sens Actuat Part A Phys* 2009; 155: 246–252.
10. Wu D, Wu L, Sun Y, et al. Rheological properties and crystallization behavior of multi-walled carbon nanotube/poly (e-caprolactone) composites. *J Polym Sci Part B Polym Phys* 2007; 453: 137–147.
11. Kashiwagi T, Grulke E, Hilding J, et al. Thermal and flammability properties of polypropylene/carbon nanotube nanocomposites. *Polymer* 2004; 45: 4227–4239.
12. Ajayan P, Stephan O, Colliex C, et al. Aligned carbon nanotube arrays formed by cutting a polymer resin–nanotube composite. *Science* 1994; 265: 1212–1214.
13. Moniruzzaman M and Winey KL. Polymer nanocomposites containing carbon nanotubes. *Macromolecules* 2006; 39: 5194–5205.
14. Zhao Y, Qiu Z and Yang W. Effect of multi-walled carbon nanotubes on the crystallization and hydrolytic degradation of biodegradable poly(l-lactide). *Compos Sci Technol* 2009; 69: 627–632.
15. Song YI, Yang CM, Kim DY, et al. Flexible transparent conducting single-wall carbon nanotube film with network bridging method. *J Colloid Interf Sci* 2008; 318: 365–371.
16. Logakis E, Pissis P, Pospiech D, et al. Low electrical percolation threshold in poly (ethylene terephthalate)/multi-walled carbon nanotube nanocomposites. *Eur Polym J* 2010; 46: 928–936.
17. Antoniadis G, Paraskevopoulos KM, Bikiaris D, et al. Non-isothermal crystallization kinetic of poly(ethylene terephthalate)/fumed silica (PET/SiO_2) prepared by in situ polymerization. *Thermochim Acta* 2010; 24: 45–52.
18. Logakis E, Pissis P, Pospiech D, et al. Low electrical percolation threshold in poly(ethylene terephthalate)/multi-walled carbon nanotube nanocomposites. *Eur Poly J* 2010; 46: 928–934.
19. Makela T, Jussila S and Kosonen H. Magnetic field alignment and electrical properties of solution cast

PET–carbon nanotube composite films. *Polymer* 2010; 50: 898–904.
20. Steinert BW and Dean DR. Magnetic field alignment and electrical properties of solution cast PET-carbon nanotube composite films. *Polymer* 2009; 1: 1–7.
21. Makela T, Jussila S, Kosonen H, et al. Utilizing roll-to-roll techniques for manufacturing source-drain electrodes for all-polymer transistors. *Synth Metal* 2005; 153: 285–288.
22. Anand KA, Agarwal US and Joseph R. Carbon nanotubes induced crystallization of poly (ethylene terephthalate). *Polymer* 2006; 47: 3976–3980.
23. Gao Y, Wang Y, Shi J, et al. Effect of functionalized MWCNTs on microstructure of PP-g-MA/OMMT/f-MWCNTs nanocomposite. *J Appl Polym Sci* 2009; 112: 2413–2424.
24. Starkweather HW, Zoller P and Jones GA. The heat of fusion of 66 nylon. *J Polym Sci Polym Phys* 1983; 21: 295–299.
25. Xu W, Ge M and He P. Nonisothermal crystallization kinetics of polypropylene/montmorillonite nanocomposites. *J Polym Sci Part B Polym Phys* 2002; 40: 408–414.
26. Chung JW, Son SB, Chun SW, et al. Thermally stable exfoliated poly(ethylene terephthalate)(PET) nanocomposites as prepared by selective removal of organic modifiers of layered silicate. *Polym Degrad Stab* 2008; 93: 252–259.
27. Kim JY, Choi HJ, Kang CS, et al. Influence of modified carbon nanotube on physical properties and crystallization behavior of poly(ethylene terephthalate) nanocomposite. *Polym Compos* 2010; 31: 858–869.
28. Avrami M. Kinetics of phase change. II Transformation-time relations for random distribution of nuclei. *J Chem Phys* 1940; 8: 212–224.
29. Sperling LH. *Introduction to physical polymer science*. New York: Wiley, 2006.
30. Jeziorny A. Parameters characterizing the kinetics of the non-isothermal crystallization of poly(ethylene terephthalate) determined by DSC. *Polymer* 1978; 19: 1142–1144.
31. Lonkar SP, Morlat-Therias S, Caperaa N, et al. Preparation and nonisothermal crystallization behavior of polypropylene/layered double hydroxide nanocomposites. *Polymer* 2009; 50: 1505–1515.
32. Ozawa T. Kinetics of non-isothermal crystallization. *Polymer* 1971; 12: 150–158.
33. Xu W, Liang G, Wang W, et al. Poly(propylene)–poly (propylene)-grafted maleic anhydride-organic montmorillonite (PP-PP-g-MAH–Org-MMT) nanocomposites. II. Nonisothermal crystallization. *J Appl Polym Sci* 2003; 88: 3093–3099.
34. Liu T, Mo Z, Wang S, et al. Nonisothermal melt and cold crystallization kinetics of poly(aryl ether ether ketone ketone). *Polym Eng Sci* 1997; 37: 568–575.
35. Goodarzi V, Jafari SH, Khonakdar HA, et al. Nonisothermal crystallization kinetics and determination of surface-folding free energy of PP/EVA/OMMT nanocomposites. *J Polym Sci Polym Phys* 2009; 47: 674–684.
36. Vassiliou AA, Papageorgiou GZ, Achilias DS, et al. Non-isothermal crystallisation kinetics of in situ prepared poly(ε-caprolactone)/surface-treated SiO_2 nanocomposites. *Macromol Chem Phys* 2007; 208: 364–376.
37. Dobreva A and Gutzow I. Activity of substrates in the catalyzed nucleation of glass-forming melts. II. Experimental evidence. *J Non-Cryst Solids* 1993; 162: 1–12.
38. Lauritzen JL and Hoffman JD. Extension of theory of growth of chain-folded polymer crystals to large undercoolings. *J Appl Phys* 1873; 44: 4340–4352.
39. Hoffman JD and Miller RL. Kinetic of crystallization from the melt and chain folding in polyethylene fractions revisited: theory and experiment. *Polymer* 1997; 38: 3151–3137.
40. Liu T, Mo Z, Wang S, et al. Isothermal melt and cold crystallization kinetics of poly(aryl ether ether ketone ketone)(PEEKK). *Eur Polym J* 1997; 33: 1405–1414.
41. Cahn JW. *Crystal growth*. New York: Pergamon Press, 1967.
42. Xu J, Srinivas S and Marand H. Equilibrium melting temperature and undercooling dependence of the spherulitic growth rate of isotactic polypropylene. *Macromolecules* 1998; 31: 8230–8242.
43. Hoffman JD and Weeks JJ. Melting process and equilibrium melting temperature of polychlorotrifluoroethylene. *Res Natl Bur Stand* 1962; 66A: 13–18.
44. Jiang XL, Luo SJ, Sun K, et al. Effect of nucleating agents on crystallization kinetics of PET. *Polym Lett* 2007; 1: 245–251.
45. Gedde UW. *Polymer physics*. London: Chapman & Hall, 1995.
46. Kissinger HE. Variation of peak temperature with heating rate in differential thermal analysis. *J Res Natl Bur Stand* 1956; 57: 217–221.
47. Vyazovkin S and Sbirrazzuoli N. Variation in activation energy of the glass transition for polymers of different dynamic fragility. *Macromol Chem Phys* 2006; 207: 1126–1130.
48. Vyazovkin S and Sbirrazzuoli N. Estimating the activation energy for non-isothermal crystallization of polymer melts. *J Therm Anal Calorim* 2003; 72: 681–686.
49. Liang H, Xie F, Guo F, et al. Non-isothermal crystallization behavior of poly(ethylene terephthalate)/poly(trimethylene terephthalate) blends. *Polym Bull* 2008; 60: 115–127.
50. Vyazovkin S and Sbirrazzuoli N. Isoconversional kinetic analysis of thermally stimulated processes in polymers. *Macromol Rapid Commun* 2004; 25: 733–738.
51. Goodarzi V, Jafari SH, Khonakdar HA, et al. An assessment of the role of morphology in thermal/thermo-oxidative degradation mechanism of PP/EVA/clay nanocomposites. *Polym Degrad Stab* 2010; 95: 859–869.
52. Goodarzi V, Monemian SA, Torabi Angaji M, et al. Improvement of thermal and fire properties of polypropylene. *J Appl Polym Sci* 2008; 110: 2971–2979.

53. Bikiaris D, Vassiliou A, Chrissafis K, et al. Effect of acid treated multi-walled carbon nanotubes on the mechanical, permeability, thermal properties and thermo-oxidative stability of isotactic polypropylene. *Polym Degrad Stab* 2008; 93: 952–967.
54. Zhang K, Hong J, Cao G, et al. The kinetics of thermal dehydration of copper (II) acetate monohydrate in air. *Thermochim Acta* 2005; 473: 145–149.
55. Burnha AK and Weese MRK. Kinetics of thermal degradation of explosive binders Viton A, Estane, and Kel-F. *Thermochim Acta* 2005; 426: 85–92.